



The effects of Co/Cu Co-doped ZnO thin films: An optical study

Dogan Akcan ^a, Sarper Ozharar ^b, Ersin Ozugurlu ^c, Lutfi Arda ^{a,*}

^a Department of Mechatronics Engineering, Faculty of Engineering and Natural Sciences, Bahcesehir University, 34349 Besiktas, Istanbul, Turkey

^b Department of Electrical-Electronics Engineering, Faculty of Engineering and Natural Sciences, Bahcesehir University, 34349 Besiktas, Istanbul, Turkey

^c Istanbul Technical University, Department of Mathematics, 34437 Maslak, Istanbul, Turkey



ARTICLE INFO

Article history:

Received 15 February 2019

Received in revised form

8 May 2019

Accepted 11 May 2019

Available online 14 May 2019

Keywords:

Sol-gel

Thin films

Optical transmission

Refractive index

Curve fitting

ZnO

ABSTRACT

In this work, a theoretical transmittance model has been used to analyze the optical characteristics, namely, the refractive index, the absorption loss, and the thickness of $Zn_{0.99-x}Cu_{0.01}Co_xO$ ($x = 0.01-0.05$, with an increment of 0.01) thin films based on their optical transmittance data. All the thin film samples are low loss and double-facet-coated substrate systems. Our model assumed the Cauchy's dispersion equation of three-term for refractive index and Lorentzian absorption profile for the extinction coefficient due to the low loss of the samples. The equations of refractive index and extinction coefficient, and the total transmittance for the thin films were derived and fitted to the experimental data in a least-squares method. The thicknesses of these sample films were found in the range of 338–355 nm. The effects of increasing cobalt concentration on the extinction coefficient have been observed.

© 2019 Elsevier B.V. All rights reserved.

1. Introduction

Optical thin films, due to their unique properties, are widely used in several areas such as automotive industry, medical equipment, communications, computers, spintronics, optoelectronics, biomaterials, data storage, energy conversion, and even in architecture [1–8]. Various film parameters like thickness, coarseness, homogeneity should be controlled accurately to fabricate thin films of a certain application. Thin films have been fabricated by various physical and chemical methods like sputtering, physical vapor deposition (PVD), pulsed laser deposition (PLD), chemical vapor deposition (CVD), molecular beam epitaxy (MBE), atomic layer deposition (ALD), spray pyrolysis, electrodeposition, metal-organic chemical vapor deposition (MOCVD) and sol-gel method [8–16]. Among these methods, sol-gel dip coating method has various advantages such as deposition under non-vacuum/ambient conditions, not requiring sophisticated equipment, highly precise and easily arranged doping ratios. Besides, unlike physical methods like MBE or sputtering, loose structure of thin films deposited by sol-gel

method is ideal for applications requiring large surface area, like sensors [2,3,7–10,15].

1.1. Double facet coated substrate structures

The sol-gel dip coating method, just like Langmuir-Blodgett and chemical bath deposition (CBD) methods, results in a thin film on both sides of the substrate material [7,17,18]. As a result, there will be two symmetric thin films on both sides of the substrate as shown in Fig. 1b.

In this paper, such a structure will be named as “Double Facet Coated Substrate” (DFCS), whereas a standard film coated on the substrate will be named as “Single Facet Coated Substrate” (SFCS) (Fig. 1a). Due to the second thin film, the interaction between the light and the DFCS is fundamentally different from the interaction between the light and the SFCS. Therefore, the widely used envelope method (Swanepoel's method) for analyzing and characterizing the thin films on a substrate is not applicable to DFCS systems.

In our earlier work, a mathematical model was developed to calculate the optical properties together with the thickness of a thin film on a DFCS based on its optical transmittance measurement [19]. This previous approach, which can be considered as a modified version of the Swanepoel's method, assumed lossless thin films on a lossless substrate. In this paper, the low loss of both the thin

* Corresponding author. Ciragan Cad. Osmanpasa Mektebi Sok., 34349 Besiktas, Istanbul, Turkey.

E-mail address: lutfi.arda@eng.bau.edu.tr (L. Arda).

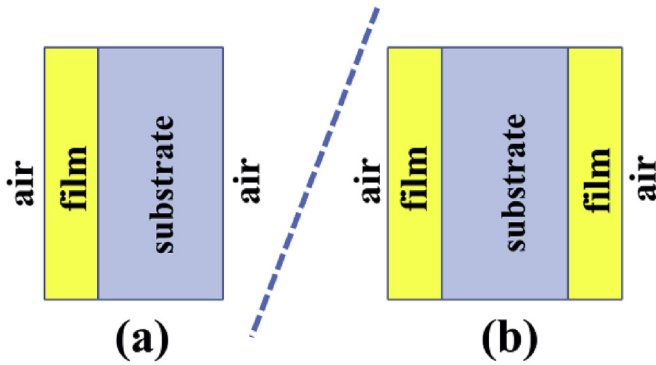


Fig. 1. (a) Single facet coated substrate (SFCS), (b) Double facet coated substrate (DFCS).

films and the substrate are included in the model.

1.2. Co/Cu co-doped zinc oxide thin films

Zinc oxide is one of the attractive materials for optoelectronic applications in the visible and infrared regions. When ZnO is doped with transition metals such as (Cu, Fe, Cr, Ni, Co, Mn, etc.), its electrical, optical, magnetic and mechanical properties change [20–25]. Especially, doping copper into zinc oxide may change the electrical and optical properties of the nanomaterials. Omri et al. showed that when Cu concentration was increased AC conductivity increased however activation energy decreased [26]. Asikuzun et al. found that the transmittance values decreased with increasing Cu doping level and 1% Cu doping ratio of thin film was the best ratio to show the smoothest surface [2]. Co doped ZnO films are known as transparent, high conductive and low-cost [27–30]. As Co concentration increased this transparency disappeared due to d-d transitions of Co ions [7 and references therein].

In this work, zinc oxide films doped with both copper and cobalt were fabricated using the sol-gel dip method. By changing the cobalt concentration from 0.01 to 0.05, five different $\text{Zn}_{0.99-x}\text{Cu}_{0.01}\text{Co}_x\text{O}$ thin films were obtained and their optical transmittance were measured between 200 and 1100 nm. The main reason for the choice of cobalt doping is the three resonant absorption peaks around 500 nm. Moreover, the optical properties such as refractive index and extinction coefficient of optical thin films were studied and analyzed for those materials on different doping ratios of cobalt to obtain the optimal configuration for the best performance. To attain this, the parametric equations of refractive index, extinction coefficient, and transmittance for the thin films were derived, then numerically calculated in a least-squares method and visualized by MATLAB code.

2. Review of theoretical transmittance model

2.1. The derivation of the optical transmittance model for a lossy DFCS structure

The well-known Fresnel reflection and transmission coefficients of the electric field between the media 1 and 2 at a normal incidence are given as follows, respectively:

$$r_{12} = \frac{\eta_1 - \eta_2}{\eta_1 + \eta_2} \quad (1)$$

$$t_{12} = \frac{2\eta_1}{\eta_1 + \eta_2} \quad (2)$$

In the above equations, η_1 and η_2 correspond to the complex refractive indices of the media 1 and 2, respectively. The complex refractive index is defined as $\eta = n + ik$ where n is the refractive index and k is the extinction coefficient which are related to each other via Kramers-Krönig relation [31].

Since the electric field reflects multiple times between the two interfaces of a thin film (air-film and film-substrate), the total reflectivity and transmissivity of the thin film are found by an infinite coherent summation of these multiple reflected electric fields, where the phase shift due to the film thickness should be included in the calculation. This wavelength-dependent phase shift results also in a wavelength-dependent transmission function. The resulting electric field reflection and transmission coefficients for an air-film-substrate (afs) system are respectively given by:

$$r_{afs} = \frac{r_{af} + r_{fs} \exp(i\theta)}{1 + r_{af}r_{fs} \exp(i\theta)} \quad (3)$$

$$t_{afs} = \frac{t_{af}t_{fs} \exp(i\theta/2)}{1 + r_{af}r_{fs} \exp(i\theta)} \quad (4)$$

where $\theta = 4\pi\eta_{film}d_{film}/\lambda$ is the complex phase shift at each round trip through the film of thickness d_{film} at the wavelength λ , and η_{film} is the complex refractive index of the thin film. However, the experimentally more relevant parameters are the intensity reflectance and transmittance, since they are real numbers and can be measured directly. These parameters are formulated in the following equations:

$$R_{afs} = r_{afs}r_{afs}^* \quad (5)$$

$$T_{afs} = \frac{n_s}{n_a} t_{afs}t_{afs}^* \quad (6)$$

where * operator denotes the complex conjugate. Note that these equations assume that the substrate thickness is semi-infinite, and the transmitted light is still inside the substrate medium. If a substrate of finite thickness is considered, then the transmittance formula, shown in Eq. (6), transforms into the well-known Swanepoel's formula [32].

In our study, a DFCS structure was considered and thus the effect of the finite substrate has been modified by including the existence of the second thin film as well as the associated losses of both thin films and the substrate.

In this analysis, there are three regions of interest where the electric field reflects multiple times as shown in Fig. 2. The region 1 is the first thin film which is sandwiched between air and the substrate. The region 2 is the finite substrate sandwiched between the two thin films. Finally, region 3 is the second thin film sandwiched between the substrate and air.

One important aspect of this analysis is that the transmittance measurements are done using a broadband light source having a short coherence length comparable with the thickness of the thin films. Therefore, for the regions 1 and 3, the acquired phase shift of the electric field due to the film thickness should be included in the reflectance and transmittance formulae, since these are based on the coherent summation of the multiple reflected electric fields.

On the other hand, the thickness of the region 2 (i.e. the substrate) is much longer compared to the coherence length of the light source, hence there will not be any interference among the multiple reflected electric fields (i.e. the acquired phase shift through the substrate is irrelevant to the total transmittance). So, the effect of the finite substrate is involved as the summation of the multiple reflected intensities instead of the electric fields. However,

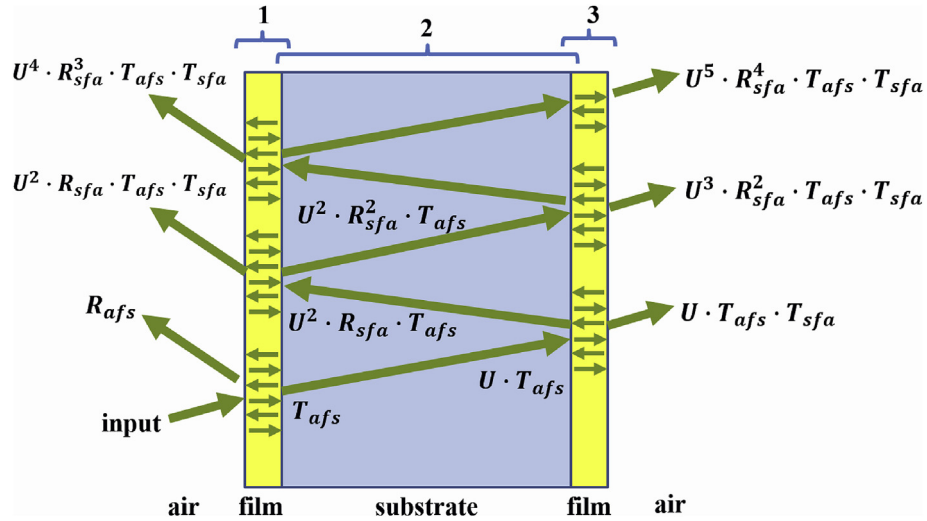


Fig. 2. The derivation of the total transmittance formula of the DFCS system.

the substrate thickness is still included in our calculations since it determines the amount of loss the light beam experiences.

As shown in Fig. 2, there is an infinite coherent summation inside the first thin film that is phase-dependent, and the transmittance, T_{afs} , was given in Eq. (6). After exiting the region 1, the light passes through the substrate and experiences an absorption loss U given as:

$$U = \text{Exp}(-\alpha_{sub} \cdot d_{sub}) \quad (7)$$

where α_{sub} is the absorption coefficient of the substrate given by $\alpha_{sub} = \frac{4\pi}{\lambda}k_{sub}$, k_s is the extinction coefficient of the substrate, and d_{sub} is the substrate thickness.

At the other end of the substrate, there is a second thin film (region 3), where another phase dependent transmission occurs (T_{sfa}). However, part of the light reflects from this second thin film with the reflection coefficient R_{sfa} , experiences the loss U again and reaches the first thin film and reflects again. As a result, it is easy to show that after each round trip through the substrate, the light acquires an additional $U^2 R_{sfa}^2$ multiplier, and the total transmittance of this DFCS system T_{system} can be calculated by the summation of all these coefficients:

$$T_{system} = T_{afs} \cdot U \cdot T_{sfa} \left(1 + U^2 R_{sfa}^2 + U^4 R_{sfa}^4 + U^6 R_{sfa}^6 + \dots \right) \quad (8)$$

Using the geometric series expansion formula, provided that $|U^2 R_{sfa}^2| < 1$, the above equation is simplified as:

$$T_{system} = \frac{T_{afs} \cdot T_{sfa} \cdot U}{1 - R_{sfa}^2 \cdot U^2} \quad (9)$$

The reader should note that if one considers a lossless substrate (i.e. $U = 1$), then Eq. (9) transforms into the improved Swanepoel's formula reported in our earlier work [19].

In a similar manner, the total reflectance of the DFCS system R_{system} can be found as follows

$$R_{system} = R_{afs} + T_{sfa} \cdot T_{afs} \cdot R_{sfa} \cdot U^2 \left(1 + U^2 R_{sfa}^2 + U^4 R_{sfa}^4 + U^6 R_{sfa}^6 + \dots \right) \quad (10)$$

and be simplified as:

$$R_{system} = R_{afs} + \frac{T_{sfa} \cdot T_{afs} \cdot R_{sfa} \cdot U^2}{1 - R_{sfa}^2 \cdot U^2} \quad (11)$$

2.2. Functional form of the complex refractive index of the thin film

The total transmittance Eq. (9) was used to determine the refractive index, loss, and the thickness of $\text{Zn}_{0.99-x}\text{Cu}_{0.01}\text{Co}_x\text{O}$ ($x = 0.01-0.05$, with an increment of 0.01) thin films prepared by the sol-gel method. For this analysis, the refractive indices of these thin films are modelled after the Cauchy's dispersion equation of three-term as follows:

$$n_{film} = A + \frac{B}{\lambda^2} + \frac{C}{\lambda^4} \quad (12)$$

Similarly, the extinction coefficients of these films are modelled after four different Lorentzian absorption profiles and a wavelength-independent term as follows:

$$k_{film} = \frac{D}{1 + \left(\frac{\lambda - \lambda_D}{w_D}\right)^2} + \frac{E}{1 + \left(\frac{\lambda - \lambda_E}{w_E}\right)^2} + \frac{F}{1 + \left(\frac{\lambda - \lambda_F}{w_F}\right)^2} + \frac{G}{1 + \left(\frac{\lambda - \lambda_G}{w_G}\right)^2} + H \quad (13)$$

where D, E, F , and G are the heights of the Lorentzian peaks, H is the wavelength-independent extinction coefficient (assumed to be zero); $\lambda_D, \lambda_E, \lambda_F$, and λ_G are the resonance wavelengths; w_D, w_E, w_F , and w_G are the corresponding absorption widths. The first three peaks (D, E, F) are chosen to model the three resonant low absorption peaks of cobalt around 500 nm as stated in Section 1.2. The fourth peak (G) was included to explain the heavy loss at shorter wavelengths. Since the overall loss at the wavelength range of

interest is very low, the Kramers-Krönig relation between the refractive index and the extinction coefficient has been omitted in this analysis.

2.3. Derivation of the substrate loss

The refractive index of the soda lime silica glass used as the substrate in our experiments was taken from the literature as [33]:

$$n_{sub} = 1.513 - 3.169 \times 10^{-3} \lambda^2 + \frac{3.962 \times 10^{-3}}{\lambda^2} \quad (14)$$

The reader should note that Eq. (9) gives the transmittance of a bare (uncoated) substrate when the film thickness is taken as zero meters ($d_{film} = 0$, i.e. no film) or when the complex refractive index of the film is taken the same as air (i.e. $\eta_{film} = \eta_{air}$). Using one of these substitutions in Eq. (9) and applying the quadratic formula, one can determine an equation for the single pass substrate absorption loss U :

$$U = \frac{-T_{as}^2 + \sqrt{T_{as}^4 + 4 \cdot R_{as}^2 \cdot T_{sub}^2}}{2 \cdot R_{as}^2 \cdot T_{sub}} \quad (15)$$

where T_{as} and R_{as} are the transmittance and reflectance of the air-substrate interface respectively, and T_{sub} is the experimental transmittance data of the bare substrate shown in Fig. 3.

After calculation of U , one can use the previously stated Eq. (7) to obtain the extinction coefficient (k_{sub}) of the soda lime silica glass substrate and the substrate thickness was directly measured as 1240 μm using a caliper.

After introducing the functional forms of n_{film} , k_{film} , and numerical values of n_{sub} and k_{sub} into Eq. (9), the total transmittance equation becomes a function of wavelength and 16 unknown parameters (3 parameters from refractive index of the thin film, 12 parameters from the extinction coefficient of the thin film, and the film thickness (d_{film})).

3. Experiment

3.1. Fabrication of thin films

To experimentally confirm the validity of our approach, a DFCS

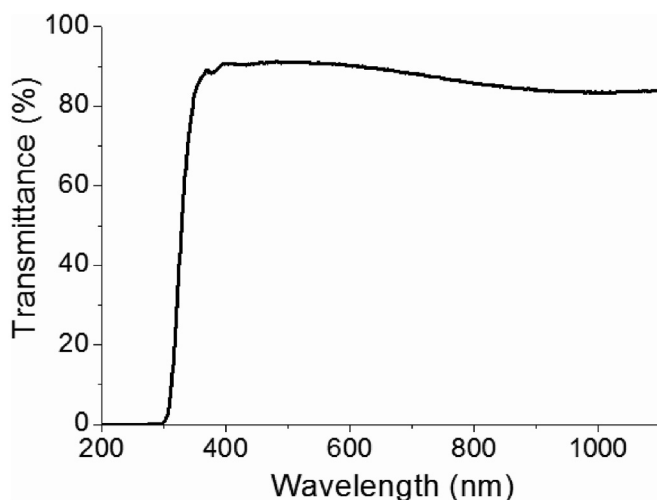


Fig. 3. . The optical transmittance of the uncoated soda lime silica glass substrate.

samples are fabricated by coating a soda lime glass substrate by Co/Cu co-doped ZnO thin films by sol-gel dip method. In this method, Zinc acetate dihydrate (ZnAc), Cobalt acetate tetrahydrate (CoAc) and Copper acetate tetrahydrate (CuAc) were used as the precursor materials and methanol (ME) and monoethanolamine (MEA) were used as solvents and sol stabilizer. ZnAc, CoAc, and CuAc are dissolved in ME with a concentration of 0.25 M and MEA is added to the solution as ZnAc, CoAc, and CuAc: MEA ratio is kept at 1:1. The final solution mixed with a magnetic stirrer at room temperature until a transparent solution was obtained. The pH of the solutions was measured by standard pH meter. The viscosity of the solutions was controlled by adding ME, see for details [2,3,7,8].

To achieve the best quality of thin films, it is important to clean extremely well the soda lime glass before deposition of the thin film. Soda lime glass is first washed with detergent, rinsed with distilled water, sonicated with 20% sulfuric acid/distilled water solution for five minutes and rinsed with distilled water again. Cleaned substrates are dried under nitrogen flow. It was found that the cleaning treatment removed all of the contaminants successfully from the surface of soda lime glass substrate.

The cleaned glass substrates were dipped into the Co/Cu co-doped ZnO solutions and then pulled through the vertical furnace at 400 °C. The film thickness on the substrate was controlled by the withdrawal speed, the number of dipping and the dilution of the solution. The process was repeated until to achieve a dense and uniform film for the desired thickness. Then, Co/Cu co-doped ZnO thin films/glass substrates are heated at 600 °C for 30 min to form a crystal structure.

3.2. Measurements

The optical transmission measurements are performed with Shimadzu UVmini 1240 UV/Vis/NIR spectrophotometer. XRD scans were recorded using a Rigaku diffractometer with Cu K α radiation. Microstructure properties of prepared samples were observed using a scanning electron microscope (JEOL, JSM-5910LV).

As stated earlier, the transmittance data were measured for five different Zn_{0.99-x}Cu_{0.01}Co_xO ($x = 0.01-0.05$, with an increment of 0.01) thin films in the range of 190–1100 nm as seen in Fig. 4a. With the increasing doping ratio of cobalt, the absorbance of the three dominant lines around 566, 614, and 661 nm was increased as well. The red shift was observed when Co concentration was increased.

4. Results and discussion

4.1. Curve fitting methodology

Our curve-fitting method only considered the range of 400–1100 nm since below 450 nm the thin films have a very high optical loss. With the increasing doping ratio of cobalt, the absorbance of the three dominant lines around 566, 607, and 656 nm was increased and these results were in good agreement with experimental data as depicted in Fig. 4b. Those three wavelength values correspond to the parameters λ_D , λ_E , and λ_F . The fourth absorption term (λ_G) in our k_{sub} formula corresponds to the strong absorption of the thin film at even shorter wavelength.

The optimization code was written in MATLAB to solve nonlinear curve-fitting (data-fitting) problem in a least-squares sense, i.e. find the parameters, say \vec{x} , that solve the problem

$$\min_{\vec{x}} \sum_{i=1}^N T_{system}(\vec{x}, \lambda_i) - TransmittanceData_i^2 \quad (16)$$

given input wavelength data λ and the observed transmittance data

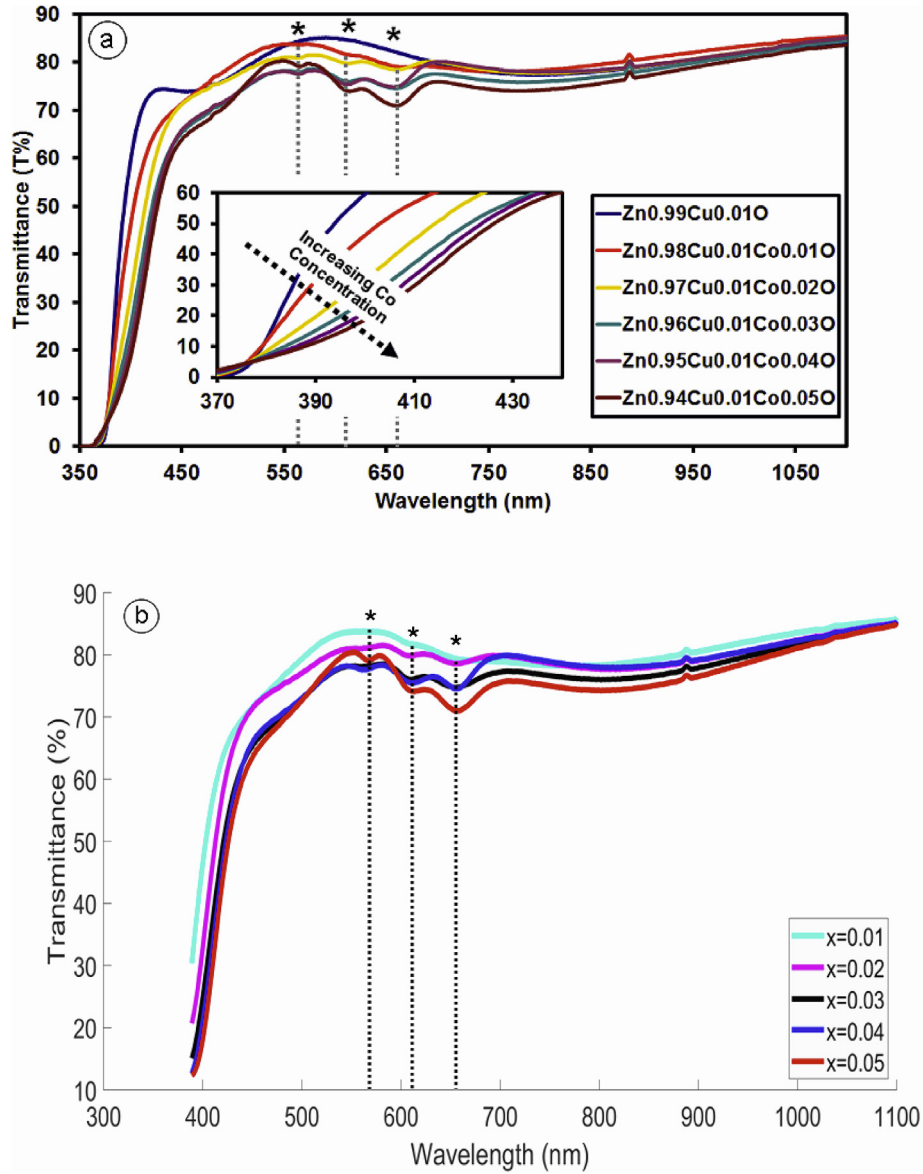


Fig. 4. . Transmittance vs. wavelength for $Zn_{0.99-x}Cu_{0.01}Co_xO$ ($x = 0.01–0.05$, with an increment of 0.01) thin films a) experimental data and b) curve fitting model.

where N is the number of data points, $T_{system}(\vec{x}, \lambda_i)$ was defined in Eq. (9), and \vec{x} is a 16-dimensional vector consisting of the unknown parameters that needs to be optimized. The initial values of these 16 parameters for the curve-fitting algorithm were determined by assuming a wavelength independent refractive index and loss (i.e. the parameters B-G are taken as zero). It was assumed that the system had no white loss. After the fitting algorithm was run, the resulting curve-fitting models together with their corresponding thin film transmittance data for five different samples are shown in Fig. 5 together with their zoomed versions.

The reader should note that the peak at 950 nm on all plots at Fig. 5 is due to the substrate, and since our model derives the substrate loss from the experimental data, the theoretical model partly fits to the peak at 950 nm intrinsically.

The curve fitting model using the least-squares method has provided the optimum values of 16 parameters which are listed in Table 1. Also, the relative error of each fitting was calculated by

$$\sqrt{\sum \left(\frac{|\text{Experimental Data} - \text{Curve Fitting}|}{|\text{Experimental Data}|} \right)^2}$$

and the resulting values were

included in Table 1 for each doping ratio of cobalt. The optimization code uses the large-scale algorithm which is a subspace trust region method and is based on the interior-reflective Newton method that is solved using the method of preconditioned conjugate gradients, see for details in Refs. [34,35].

4.2. Determined film parameters

Using the optimized A, B, C values from Table 1, the corresponding dispersion relation (Eq. (12)) for each thin film plot was shown in Fig. 6.

As seen in Fig. 6, the average refractive index increases as the Co concentration increases. However, at $x = 0.04$ a drop has been observed in the refractive index, which then increases again with increasing x value. This unexpected reduction on refractive index requires further investigation. Also, the extinction coefficients for each film can be plotted in a similar way based on Eq. (13) using the values from Table 1 as in Fig. 7.

As seen in Fig. 7, the extinction coefficient k_{film} values increase as

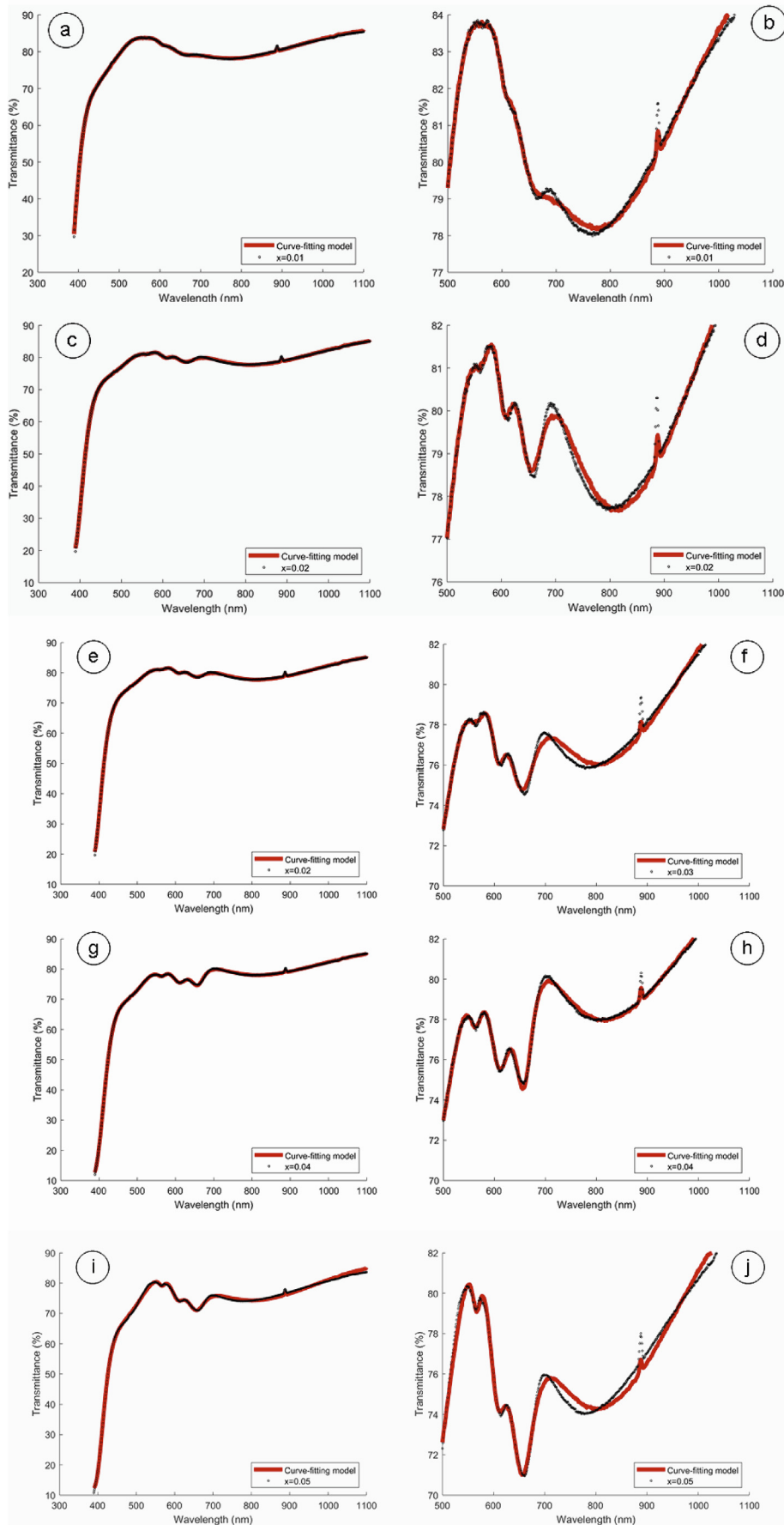
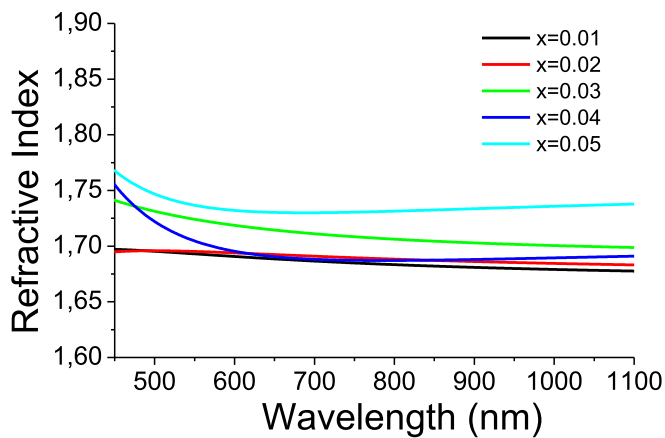
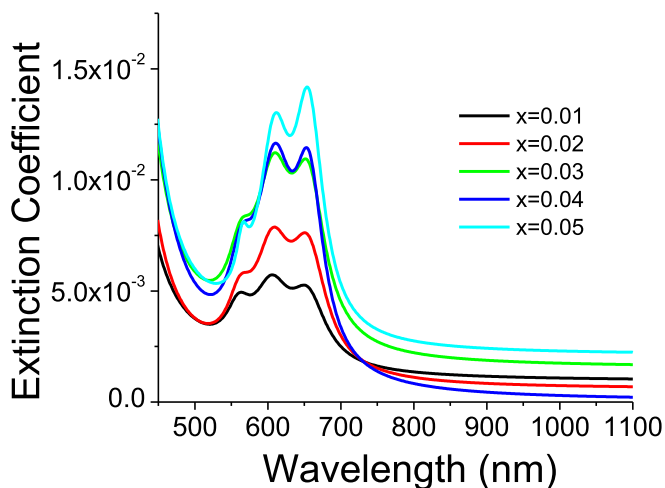


Fig. 5. Experimental transmittance data together with the theoretical curve fittings of $\text{Zn}_{0.99-x}\text{Cu}_{0.01}\text{Co}_x\text{O}$ thin film (on the left column), and the zoomed graphs (on the right column): a) and b) $x = 0.01$, c) and d) $x = 0.02$, e) and f) $x = 0.03$, g) and h) $x = 0.04$, i) and j) $x = 0.05$.

Table 1The curve-fitting model parameters for five thin film $\text{Zn}_{0.99-x}\text{Cu}_{0.01}\text{Co}_x\text{O}$ ($x = 0.01–0.05$, with an increment of 0.01) transmittance data.

	$\text{Zn}_{0.98}\text{Cu}_{0.01}\text{Co}_{0.01}\text{O}$	$\text{Zn}_{0.97}\text{Cu}_{0.01}\text{Co}_{0.02}\text{O}$	$\text{Zn}_{0.96}\text{Cu}_{0.01}\text{Co}_{0.03}\text{O}$	$\text{Zn}_{0.95}\text{Cu}_{0.01}\text{Co}_{0.04}\text{O}$	$\text{Zn}_{0.94}\text{Cu}_{0.01}\text{Co}_{0.05}\text{O}$
A	1.7039	1.6901	1.7411	1.7033	1.7778
B	−0.02	0.0033	−0.02	−0.02	−0.02
C	0.0036	−0.0003	0.0048	0.0062	0.0043
D	0.0012	0.0026	0.0038	0.0029	0.0025
E	0.0007	0.0037	0.0048	0.0083	0.0081
F	0.0047	0.0061	0.0087	0.0079	0.0117
G	0.1138	0.0652	0.0787	0.0817	0.0855
w_D (μm)	0.0293	0.0287	0.0302	0.0198	0.0112
w_E (μm)	0.0127	0.0226	0.0207	0.0309	0.0242
w_F (μm)	0.0726	0.0392	0.0404	0.0239	0.0321
w_G (μm)	0.0213	0.024	0.0277	0.0278	0.0246
λ_D (μm)	0.5644	0.5659	0.5675	0.5642	0.5669
λ_E (μm)	0.6044	0.6061	0.6073	0.6101	0.6078
λ_F (μm)	0.6417	0.6523	0.6529	0.6575	0.6561
λ_G (μm)	0.38143	0.3864	0.3863	0.3851	0.3920
Film Thickness (μm)	0.3414	0.3535	0.3458	0.3552	0.3383
Substrate Thickness (μm)	1240	1240	1240	1240	1240
Relative Error	1.781×10^{-3}	2.235×10^{-3}	3.29×10^{-3}	1.881×10^{-3}	6.437×10^{-3}

**Fig. 6.** Refractive index vs. wavelength for $\text{Zn}_{0.99-x}\text{Cu}_{0.01}\text{Co}_x\text{O}$ ($x = 0.01–0.05$, with an increment of 0.01) thin films.**Fig. 7.** Extinction coefficient vs. wavelength for $\text{Zn}_{0.99-x}\text{Cu}_{0.01}\text{Co}_x\text{O}$ ($x = 0.01–0.05$, with an increment of 0.01) thin films.

the doping ratio of cobalt increases.

The X-ray scan of the Cu/Co co-doped ZnO ($x = 0.01–0.05$) thin film on glass substrate was illustrated in Fig. 8. The scan shows that there is a dominant peak which is the (002) reflection of ZnO thin films. It is c-axis oriented with significant intensity. The thin films are observed using a scanning electron microscope to verify our calculated thickness values. The cross-sectional SEM measurements revealed the thickness of the $\text{Zn}_{0.98}\text{Cu}_{0.01}\text{Co}_{0.01}\text{O}$ thin film as approximately 338 nm as shown in Fig. 9c, which is in a very good agreement with the predicted value of 341.4 nm by our method. The relative error is 1%. In other words, the thickness of the thin films may be measured more accurately. Textured smooth, crack-free and pinhole-free $\text{Zn}_{0.99-x}\text{Cu}_{0.01}\text{Co}_x\text{O}$ (002) thin film could be grown on glass substrates by using the sol-gel dip-coating process. Fig. 9a and b show the SEM surface morphology of $\text{Zn}_{0.98}\text{Cu}_{0.01}\text{Co}_{0.01}\text{O}$ thin film. The film depicts homogeneous surface with uniformly distributed grains. Energy Dispersive Spectroscopy (EDS) spectrum of $\text{Zn}_{0.98}\text{Cu}_{0.01}\text{Co}_{0.01}\text{O}$ was plotted in Fig. 9c. As shown in Fig. 9c, Zn, Cu, Co, and O peaks were clearly observed.

5. Conclusion

In this work, a standard transmittance model has been used to characterize the optical properties of five different $\text{Zn}_{0.99-x}\text{Cu}_{0.01}\text{Co}_x\text{O}$ ($x = 0.01–0.05$) thin films with varying dopant ratios of cobalt using the sol-gel technique. Since the thin films were double-facet coated the model has been modified to account the effect of the secondary surface. The refractive index was assumed as a Cauchy function and the losses were taken as having Lorentzian line-shape neglecting the Kramers-Krönig relation due to the low loss. We assumed that the white loss in the system was neglected. The calculated and experimentally measured thin film thicknesses are in good agreement with a relative error of 1%. Our simulations showed that film thicknesses were in the range of 338–355 nm. The average refractive index increases as the Co concentration increases. However, at $x = 0.04$ a drop has been observed in the refractive index, which then increases again with increasing x value. This unexpected reduction on refractive index requires further investigation. The curve fitting model used for transmittance data had a relative error of 0.312%, i.e. the order of accuracy was third. The absorption peaks that we found in our simulations were in good agreement with the experimental data.

The X-Ray diffractions show that a strong peak of $\text{Zn}_{0.99}$

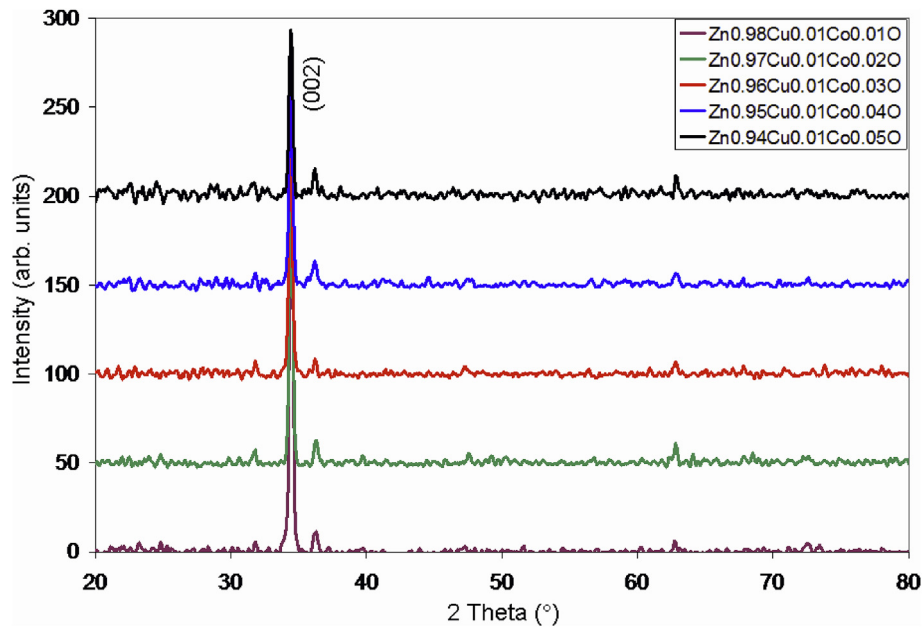


Fig. 8. XRD patterns of $\text{Zn}_{0.99-x}\text{Cu}_{0.01}\text{Co}_x\text{O}$ ($x = 0.01, 0.02, 0.03, 0.04,$ and 0.05) thin films.

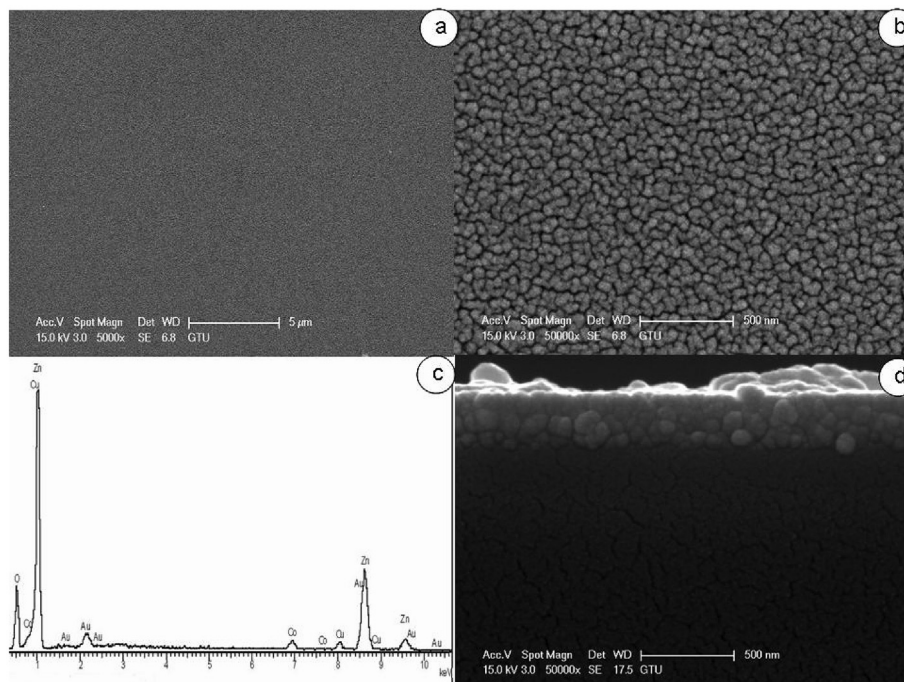


Fig. 9. a) and b) SEM images, c) EDS image, and d) cross section of $\text{Zn}_{0.98}\text{Cu}_{0.01}\text{Co}_{0.01}\text{O}$ thin film.

$\text{Zn}_{0.99-x}\text{Cu}_{0.01}\text{Co}_x\text{O}$ ($x = 0.01–0.05$) thin film (002) appears which matches with the hexagonal ZnO lattice. The cross-sectional SEM measurements revealed the thickness of the $\text{Zn}_{0.98}\text{Cu}_{0.01}\text{Co}_{0.01}\text{O}$ thin film as approximately 338 nm which is in a very good agreement with the predicted value of 341.4 nm by our method. Dense, crack-free and pinhole-free $\text{Zn}_{0.99-x}\text{Cu}_{0.01}\text{Co}_x\text{O}$ ($x = 0.01–0.05$) (002) thin film could be grown on glass substrates by using the sol–gel dip-coating process. Fig. 9a and b show the SEM surface morphology of $\text{Zn}_{0.98}\text{Cu}_{0.01}\text{Co}_{0.01}\text{O}$ thin film. The film depicts homogeneous surface with uniformly distributed grains.

Acknowledgement

The presented work was supported by the Research Fund of Bahcesehir University, Istanbul, Turkey (Project No. BAU-BAP.2018.02.16).

References

- [1] J.A. Dobrowolski, in: R.F. Hummel, K.H. Guenther (Eds.), *Thin Films for Optical Coatings*, McGraw-Hill, New York, 1995, pp. 5–35.
- [2] E. Asikuzun, O. Ozturk, L. Arda, C. Terzioğlu, *Preparation, growth and*

- characterization of nonvacuum Cu-doped ZnO thin films, *J. Mol. Struct.* 1165 (1) (2018).
- [3] D. Akcan, A. Gungor, L. Arda, Structural and optical properties of Na-doped ZnO films, *J. Mol. Struct.* 1161 (2018) 299.
- [4] J.G. Lu, Z.Z. Ye, Y.J. Zeng, L.P. Zhu, L. Wang, J. Yuan, Q.L. Liang, Structural, optical, and electrical properties of (Zn,Al)O films over a wide range of compositions, *J. Appl. Phys.* 100 (2006), 073714.
- [5] S.A. Wolf, D. Awschalom, R.A. Buhrman, J.M. Daughton, S.V. Molnar, M.L. Roukes, A.Y. Chtchelkanova, D.M. Treger, Spintronics: a spin-based electronics vision for the future, *Science* 294 (2001) 1488.
- [6] Y. Ammaih, A. Abderrazak, B. Hartiti, A. Ridah, P. Thevenin, M. Siadat, Structural, optical and electrical properties of ZnO:Al thin films for optoelectronic applications, *Opt. Quant. Electron.* 46 (2014) 229–234.
- [7] Z.K. Heiba, L. Arda, XRD, XPS, optical, and Raman investigations of structural changes of nano Co-doped ZnO, *J. Mol. Struct.* 1022 (2012) 167–171.
- [8] E. Asikuzun, O. Ozturk, L. Arda, C. Terzioğlu, Microstructural and electrical characterizations of transparent Er-doped ZnO nano thin films prepared by sol-gel process, *J. Mater. Sci. Mater. Electron.* 28 (19) (2017) 14314–14322.
- [9] N. Kiling, S. Öztürk, L. Arda, A. Altindal, Z.Z. Öztürk, Structural, electrical transport and NO₂ sensing properties of Y-doped ZnO thin films, *J. Alloys Compd.* 536 (2012) 138–144.
- [10] E. Asikuzun, O. Ozturk, L. Arda, A.T. Tasci, F. Kartal, C. Terzioğlu, High-quality c-axis oriented non-vacuum Er doped ZnO thin films, *Ceram. Int.* 42 (7) (2016) 8085–8091.
- [11] N.C. Mamani, R.T. da Silva, A.O. de Zevallos, et al., On the nature of the room temperature ferromagnetism in nanoparticulate co-doped ZnO thin films prepared by EB-PVD, *J. Alloys Compd.* (695) (2017) 2682–2688.
- [12] P. Shokeen, A. Jain, A. Kapoor, Plasmonic ZnO/p-silicon heterojunction solar cell, *Opt. Mater.* 67 (2017) 32–37.
- [13] Z. Chen, X. Chen, S. Chu, et al., Ultraviolet to violet lasing from Cd_xZn_{1-x}O microdisks produced by chemical vapor deposition, *Opt. Mater.* 72 (2017) 459–463.
- [14] J.W. Mares, F.R. Ruhge, A.V. Thompson, et al., Optical and morphological properties of MBE grown wurtzite Cd_xZn_{1-x}O thin films, *Opt. Mater.* 30 (2) (2007) 346–350.
- [15] S. Ghosh, U.M.K. Kumar, B.N.S. Bhaktha, Heat-treatment controlled structural and optical properties of sol-gel fabricated Eu: ZnO thin films, *Opt. Mater.* 64 (2017) 288–294.
- [16] J.L. Zhao, X.W. Sun, H. Ryu, et al., Thermally stable transparent conducting and highly infrared reflective Ga-doped ZnO thin films by metal organic chemical vapor deposition, *Opt. Mater.* 33 (6) (2011) 768–772.
- [17] R.S. Singh, S. Bhushan, A.K. Singh, S.R. Deo, Characterization and optical properties of Cdse nano-Crystalline thin films, *Digest J. Nanomater. Biostruct.* 6 (2) (2011) 403–412.
- [18] L. Arda, Z.K. Heiba, Rare-earth mixed oxide thin films as 100% lattice match buffer layers for YBa₂Cu₃O_{7-x} coated conductors, *Thin Solid Films* 518 (12) (2010) 3345–3350.
- [19] S. Ozharar, D. Akcan, L. Arda, Determination of the refractive index and the thickness of double side coated thin films, *J. Optoelectron. Adv. Mater.* 18 (1–2) (2016) 65–69.
- [20] A. Guler, L. Arda, N. Dogan, C. Boyraz, E. Ozugurlu, The annealing effect on microstructure and ESR properties of (Cu/Ni) co-doped ZnO nanoparticles, *Ceram. Int.* 45 (2) (2019) 1737–1745.
- [21] Z.K. Heiba, L. Arda, M.B. Mohammed, Y.M. Nasser, N. Dogan, Effect of annealing temperature on structural and magnetic properties of Zn_{0.94}Co_{0.05}Cu_{0.01}O, *J. Supercond. Nov. Magnetism* 26 (12) (2013) 3487–3493.
- [22] Z.K. Heiba, L. Arda, M.B. Mohamed, M.A. Al-Jalali, N. Dogan, Structural and magnetic properties of (Al/Mg) Co-doped nano ZnO, *J. Supercond. Nov. Magnetism* 26 (11) (2013) 3299–3304.
- [23] E. Asikuzun, A. Donmez, L. Arda, O. Cakiroglu, O. Ozturk, D. Akcan, M. Tosun, S. Ataoglu, C. Terzioğlu, Structural and mechanical properties of (Co/Mg) co-doped nano ZnO, *Ceram. Int.* 41 (5) (2015) 6326–6334. Part A.
- [24] K. Ueda, H. Tabata, T. Kawai, Magnetic and electric properties of transition-metal-doped ZnO films, *Appl. Phys. Lett.* 79 (2001) 988–990.
- [25] M. Tosun, S. Ataoglu, L. Arda, O. Ozturk, E. Asikuzun, D. Akcan, O. Cakiroglu, Structural and mechanical properties of ZnMgO nanoparticles, *Mater. Sci. Eng. A* 590 (2014) 416–422.
- [26] K. Omri, A. Bettaibi, K. Khirouni, L. El Mir, The optoelectronic properties and role of Cu concentration on the structural and electrical properties of Cu doped ZnO nanoparticles, *Phys. B Condens. Matter* 537 (2018) 167–175.
- [27] S. Benramache, B. Benhaoua, Influence of substrate temperature and Cobalt concentration on structural and optical properties of ZnO thin films prepared by Ultrasonic spray technique, *Superlattice. Microst.* 52 (2012) 807–815.
- [28] S. Vijayakumar, S.H. Lee, K.S. Ryu, Hierarchical CuCo₂O₄ nanobelts as a supercapacitor electrode with high areal and specific capacitance, *Electrochim. Acta* 182 (2015) 979–986.
- [29] A. Amri, Z.T. Jiang, T. Pryor, C.Y. Yin, Z. Xie, N. Mondinos, Optical and mechanical characterization of novel cobalt-based metal oxide thin films synthesized using sol-gel dip-coating method, *Surf. Coating. Technol.* 207 (2012) 367–374.
- [30] A. Amri, X. Duan, C.Y. Yin, Z.T. Jiang, M.M. Rahman, T. Pryor, Solar absorptance of copper-cobalt oxide thin film coatings with nano-size, grain-like morphology: optimization and synchrotron radiation XPS studies, *Appl. Surf. Sci.* 275 (2013) 127–135.
- [31] S. John, Toll, Causality and the dispersion relation: logical foundations, *Phys. Rev.* 104 (1956) 1760–1770.
- [32] Z. Knittl, *Optics of Thin Films*, Wiley, New York, 1971.
- [33] M. Rubin, Optical properties of soda lime silica glasses, *Sol. Energy Mater.* 12 (1985) 275–288.
- [34] T.F. Coleman, Y. Li, An interior, trust region approach for nonlinear minimization subject to bounds, *SIAM J. Optim.* 6 (1996) 418–445.
- [35] T.F. Coleman, Y. Li, On the convergence of reflective Newton methods for large-scale nonlinear minimization subject to bounds, *Math. Program.* 62 (2) (1994) 189–224.